Neuroradiology (2013) 55:751–758
DOI 10.1007/s00234-013-1169-2

INTERVENTIONAL NEURORADIOLOGY

Flow diverter effect on cerebral aneurysm hemodynamics: an in vitro comparison of telescoping stents and the Pipeline

Breigh N. Roszelle · L. Fernando Gonzalez · M. Haithem Babiker · Justin Ryan · Felipe C. Albuquerque · David H. Frakes

Received: 28 September 2012 / Accepted: 4 March 2013 / Published online: 21 March 2013

Abstract
Introduction Flow diverting devices and stents can be used to treat cerebral aneurysms too difficult to treat with coiling or craniotomy and clipping. However, the hemodynamic effects of these devices have not been studied in depth. The objective of this study was to quantify and understand the fluid dynamic changes that occur within bifurcating aneurysms when treated with different devices and configurations.
Methods Two physical models of bifurcating cerebral aneurysms were constructed: an idealized model and a patient-specific model. The models were treated with four device configurations: a single low-porosity Pipeline embolization device (PED) and one, two, and three high-porosity Enterprise stents deployed in a telescoping fashion. Particle image velocimetry was used to measure the fluid dynamics within the aneurysms; pressure was measured within the patient-specific model.
Results The PED resulted in the greatest reductions in fluid dynamic activity within the aneurysm for both models. However, a configuration of three telescoping stents reduced the fluid dynamic activity within the aneurysm similarly to the PED treatment. Pressure within the patient-specific aneurysm did not show significant changes among the treatment configurations; however, the pressure difference across the untreated vessel side of the model was greatest with the PED.
Conclusion Treatment with stents and a flow diverter led to reductions in aneurysmal fluid dynamic activity for both idealized and patient-specific models. While the PED resulted in the greatest flow reductions, telescoping high-porosity stents performed similarly and may represent a viable treatment alternative in situations where the use of a PED is not an option.

Keywords Aneurysm · Blood flow · Flow diverter · Particle image velocimetry · Pipeline

Introduction

The use of endovascular cerebral aneurysm treatments has greatly increased over the past decade due to their less invasive nature and increased effectiveness in comparison to traditional craniotomy and clipping [1–3]. As the most common endovascular technique, coil embolization is considered by many to be the gold standard for cerebral aneurysm treatment [4]. However, there are cases where treatments using either coiling or craniotomy and clipping are difficult, including fusiform, dissecting (blister), and giant intracranial aneurysms. For these difficult cases, sequential porous stents delivered in a "telescopic" fashion (stent-in-stent technique) have been used to alter flow within aneurysms [5]. This is known as the endoluminal approach because devices, such as stents, are deployed directly into the lumen of the diseased parent vessel in order to divert

This paper was presented in part at the ASME Summer Bioengineering Meeting in June 2012.

B. N. Roszelle (✉) · M. H. Babiker · J. Ryan · D. H. Frakes
School of Biological and Health Systems Engineering, Arizona State University, P.O. Box 879709, Tempe, AZ 85287-9709, USA
e-mail: broszelle@gmail.com

L. F. Gonzalez
Department of Neurological Surgery, Jefferson Medical College, Philadelphia, PA, USA

F. C. Albuquerque
Barrow Neurological Institute, St. Joseph's Hospital and Medical Center, Phoenix, AZ, USA

D. H. Frakes
School of Electrical, Computer, and Energy Engineering, Arizona State University, Tempe, AZ, USA

flow away from the aneurysm. The flow diversion technique promotes stasis within the aneurysm and subsequent thrombosis with endothelialization of the arterial defect along the stent wall at the aneurysm neck [6]. Endoluminal therapy has the potential advantage of occluding the aneurysm without creating any mass effect from coils, which can be deleterious especially during treatment of large aneurysms near the cranial nerves [7 ,8]. The hemodynamic and biologic effects of the flow-diverting stents include: (a) redirecting flow away from an aneurysm; (b) reconfiguring the anatomy of the parent vessel, thus changing the anatomy of the parent vessel–aneurysm complex and aneurysm inflow/outflow zone; and (c) stimulation of arterial endothelium, providing a bridging scaffold as a nidus to support neointimal growth over the aneurysm neck defect [9].

The stents used for the telescoping technique are high-porosity intracranial stents, which were originally developed to act as structural support for coil embolization [10]. The first endoluminal flow-diverting device designed especially for intracranial aneurysms and approved in the USA is the Pipeline embolization device (PED; ev3, Irvine, CA). The PED consists of a low-porosity mesh cylinder composed of braided filaments of platinum and cobalt. Because of its unique design, the PED affords coverage of the arterial defect of approximately 30–35 % of the surface area. This is an increase over single high-porosity stents, such as the Neuroform stent (Stryker, Freemont, CA) or Enterprise stent (Cordis Endovascular, Miami Lakes, FL), which only provide approximately 10 % coverage [11]. While the PED has received praise over the past few years for success in occluding aneurysms, recent studies show that 2 % of cases still resulted in severe hemorrhagic complications, which likely relate to hemodynamic factors [12].

Many previous studies have observed the hemodynamic effects of stents and other flow-diverting devices. For example, an in vitro study by Canton et al. [13] demonstrated that progressive overlapping stents decreased the vorticity, wall shear stress, and peak velocities within the aneurysm, thus facilitating aneurysm thrombosis. Additionally, a previous in vitro study by our group investigated the effects of telescoping low-porosity stents and the PED on an idealized sidewall aneurysm and found that the flow velocities within the aneurysm were reduced up to 54 % with flow diverter treatment [14]. Previous computational studies have also found that the stent-in-stent technique leads to fluid dynamic changes in the aneurysmal sac that promote stasis [13 ,15]. However, the effects of different flow diverter configurations on aneurysmal hemodynamics remain largely unknown.

The objective of this study was to compare the fluid dynamics associated with cerebral aneurysm treatment using the PED to those resulting from treatment with sequential telescoping high-porosity stents. Toward that end, particle image velocimety (PIV) was used as a flow visualization and quantification tool in both an idealized and a patient-specific, anatomical cerebral aneurysm model. The overall goal of the study was to obtain a better understanding of the effects that different stent and flow diverter configurations have on aneurysm hemodynamics in order to improve upon their current and future use as treatment tools.

Methods

Modeling

Two aneurysm models were treated with stents and a flow diverter in this study. The first was an idealized basilar tip aneurysm model that was designed using dimensions from average patient data. For the idealized model, the parent and branch vessels were each 4 mm in diameter and the diameter and neck of the aneurysm were 3.5 and 3.1 mm, respectively. A computational model of the idealized aneurysm was used to make a pot metal core with computer numerical-controlled cutting. Sylgard 184® silicon elastomere (Dow Corning, Midland, MI) was molded around the metal core, which was then melted out, leaving an optically clear, lost core model to be used for the in vitro experiments.

The second model was built from a patient-specific geometry and was constructed using a different process. The patient geometry for the model was identified in a database of computerized tomography images at the Barrow Neurological Institute because it was both representative of common cerebral aneurysms and contained structural similarities to the idealized case. The image data were enhanced and segmented with custom code in MATLAB (MathWorks, Natick, MA) [16 ,17] before being reconstructed to form a 3D computational model using Mimics software (Materialize, Ann Arbor, MI). Next, rapid prototyping was used to print the patient-specific core from a dissolvable composite material using a ZPrinter 650 RP system (Z Corporation, Burlington, MA). The printed model was then used to recast a refined metallic core. Finally, the core was cast in urethane and the metallic core was melted out, producing a lost core model for experimentation.

Device deployment

Each model was treated with four different device configurations: a single Enterprise stent (one-stent), two telescoping Enterprise stents (two-stent), three telescoping Enterprise stents (three-stent), and a PED. Experiments were also performed on the untreated models for comparison.

Flow measurement and analysis

Models were connected to a flow loop with flexible polyvinyl chloride tubing. A blood analog fluid was driven

through the loop by a Compuflow 1000 piston pump (Shelley Medical, Toronto, ON, Canada). The fluid comprised water, aqueous sodium iodide, and glycerol. The solution was configured to have a viscosity of 3.16 cP at a 25 °C operating temperature; the amount of sodium iodide in the solution was varied as needed to match the refractive index of either the Sylgard 184® (for the idealized model) or urethane (for the patient-specific model). Eight-micrometer fluorescent particles (Thermo Scientific, Waltham, MA) were seeded into the fluid to facilitate PIV experimentation. Steady and average pulsatile flow conditions were investigated at flow rates of 3, 4, and 5 ml/s. During pulsatile flow, a vertebral flow waveform from the literature was used [18].

A Flowmaster 3D stereo PIV system (LaVision, Ypsilanti, MI) was used for the PIV experiments. The system included a 532-nm wavelength Solo PIV III dual-cavity pulsed YAG laser (New Wave Research, Fremont, CA) and two Imager Intense cross-correlation CCD cameras. The laser light sheet used for slice selection was 0.5 mm thick. The laser illuminated the fluorescent particles in the working fluid, which experience peak excitation and emission at 542 and 618 nm, respectively. Because stents can cause laser reflections, low-pass optical filters with a 572-nm cutoff (Omega Optical, Brattle Bro, VT) were installed on the cameras to block reflections while allowing the particles to be imaged.

Three planes of data were acquired in the idealized model: the middle plane and two planes displaced orthogonally from the centerline by ±0.5 mm in either direction. Because the geometry of the patient-specific model was not as symmetric, five planes were taken throughout the model to thoroughly sample the flow field. The five planes spanned across the aneurysm and were also 0.5 mm apart.

During PIV acquisition, 200 image pairs were obtained at a rate of 5 Hz for each plane at each flow rate. DaVis software (LaVision) was then used to calculate flow velocity vectors with a cross-correlation algorithm. Interrogation windows with an initial size of 64×64 pixels and a final size of 16×16 pixels were used with a 50 % overlap of neighboring windows. Our methods are described in detail by Babiker et al. [19].

A single velocity flow field was averaged within each measurement plane and flow condition. A mask was then applied to the aneurysmal domain within each plane, and the root-mean-squared velocity magnitude (V_{RMS}) was calculated for the aneurysmal velocity vectors throughout all of the planes. V_{RMS} was calculated using the following equation:

$$V_{rms} = \sqrt{\frac{1}{n}\sum_{i=1}^{n} |V_i|^2}$$

where n is the number of data points within the measurement area and V_i is the flow velocity magnitude at point i. Note that V_{RMS} within the aneurysmal measurement area is representative of the fluid dynamic activity within the aneurysm, so a reduction in aneurysmal V_{RMS} indicates a reduction in the overall fluid dynamic activity within the aneurysm. Our selection of V_{RMS} as a measurement metric is due to it being inherently spatial normalized and it represents the flow of the entire volume as opposed to focusing on one direction, allowing us to quantify the complex flow field.

Pressure measurement and analysis

Pressure measurements were taken within the aneurysmal sac and at the model inlet and untreated outlet of the patient-specific model. Pressure was only measured in the patient-specific model due to material limitations of the idealized model. Measurements were taken using a fluid-filled pressure transducer (Harvard Apparatus, Holliston, MA). In order to obtain measurements within the aneurysm, a very small tap was microdrilled into the model and a microcatheter (outer diameter, 0.4 mm) was threaded into the aneurysm. The location of the pressure tap was selected based on ease of construction, lack of interference with PIV measurements, and desired location within the aneurysm. In order to prevent model leakage, the catheter entrance was sealed with silicone. To measure pressure changes across the entire model, taps were also made in connective tubing at the model inlet and outlet. The pressure transducer was connected to an amplifier unit (Harvard Apparatus) and measurements were recorded using LabVIEW Signal Express (National Instruments, Austin, TX).

Measurements were taken for 12 continuous seconds at all flow rates and under steady and pulsatile flow conditions. For the steady flow rates, an average pressure was calculated from the 12-s sample. For the pulsatile flow rates, ten full cycles were selected from the 12-s sample and averaged to generate a single average pressure curve for the entire cycle.

Results

Flow

Flow results are presented in Figs. 1 and 2 as bar graphs of the V_{RMS} within the aneurysm, for each deployment and for the idealized and patient-specific model, respectively. The percentage change between the untreated case and each deployment configuration is also highlighted in Figs. 1 and 2.

As shown in Fig. 1, V_{RMS} within the aneurysm decreased after each sequential stent placement in the idealized model. There was one exception for pulsatile flow at 5 ml/s, where the two-stent deployment resulted in a 3 % increase in V_{RMS} as compared to the one-stent deployment. The average

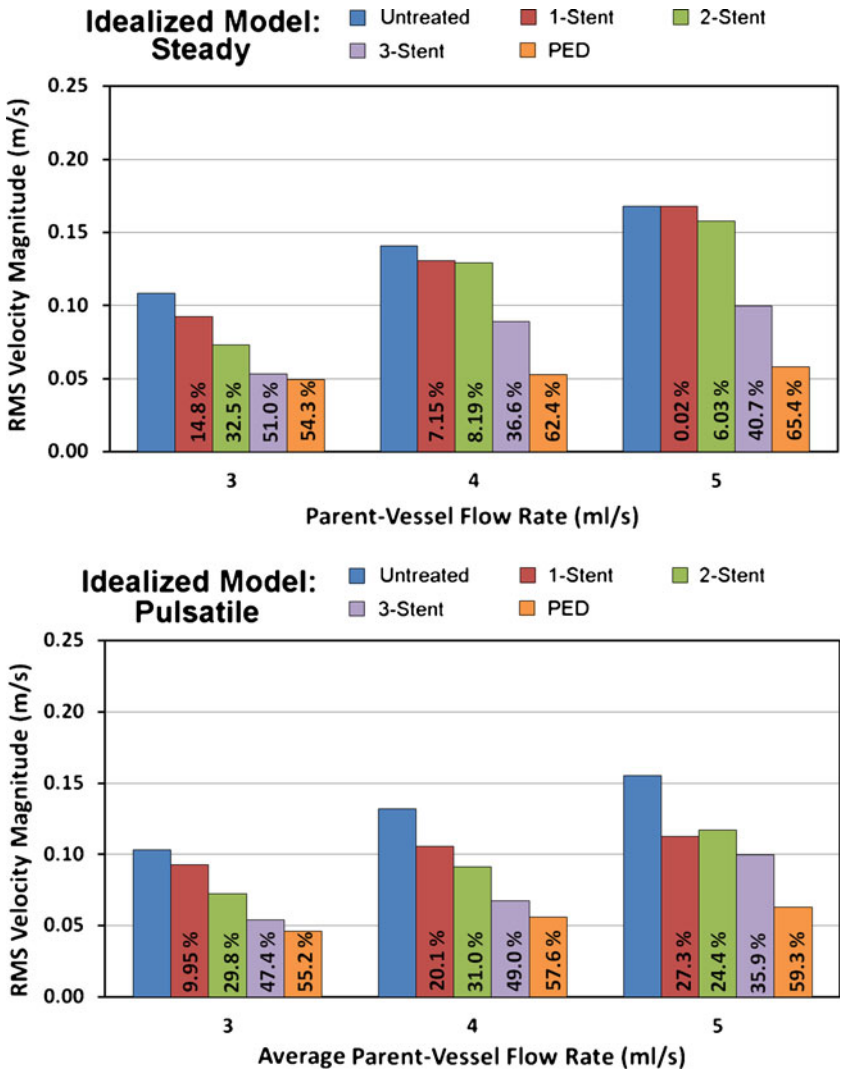

Fig 1 V_{RMS} within the aneurysm of the idealized model for each flow rate and treatment. In each case, treatment reduced the V_{RMS} within the aneurysm; however, the PED was the most effective for all flow rates

reductions in V_{RMS} across all three flow rates, as compared to the untreated case, were 7.3, 15.6, and 42.7 % for one-, two-, and three-stent deployments, respectively. Reductions for the PED were greatest across all flow rates, with an average V_{RMS} reduction of 60.7 % compared to the untreated model.

While Fig. 2 shows reductions in V_{RMS} within the aneurysm of the patient-specific model after each stent deployment, the reductions were considerably smaller than those observed in the idealized case. Also, the reductions within the patient-specific model did not follow the sequential pattern observed in the idealized case. During steady flow, the one- and two-stent deployments resulted in similar V_{RMS} reductions, 10.1 and 10.9 % on average, respectively, as compared to the untreated case. Furthermore, placement of a second stent led to an increase in V_{RMS} under pulsatile flow conditions. In comparison to the untreated case, V_{RMS} was reduced by an average of 16.2 % across all flow rates after the one-stent deployment. When the two-stent deployment was performed, the average reduction was only 8.7 %. After the three-stent deployment, V_{RMS} reductions returned to an average of 16 %. The PED led to the greatest V_{RMS} reductions for all parent vessel flow rates examined, averaging 24.3 and 19.4 % at steady and pulsatile conditions, respectively.

Pressure

For each treatment configuration, pressure within the aneurysm fluctuated within 1 or 2 mmHg as the parent vessel flow rate increased. Also, there was no significant difference in intra-aneurysmal pressure between each treatment configuration; however, overall pressure differences across the model varied noticeably among treatments. As shown in Fig. 3, the pressure difference, which is the change in pressure from the inlet vessel to the untreated outlet vessel, increased after each sequential stent deployment. The PED caused the greatest pressure difference in comparison to the untreated case, which was nearly double that observed for the three-stent deployment.

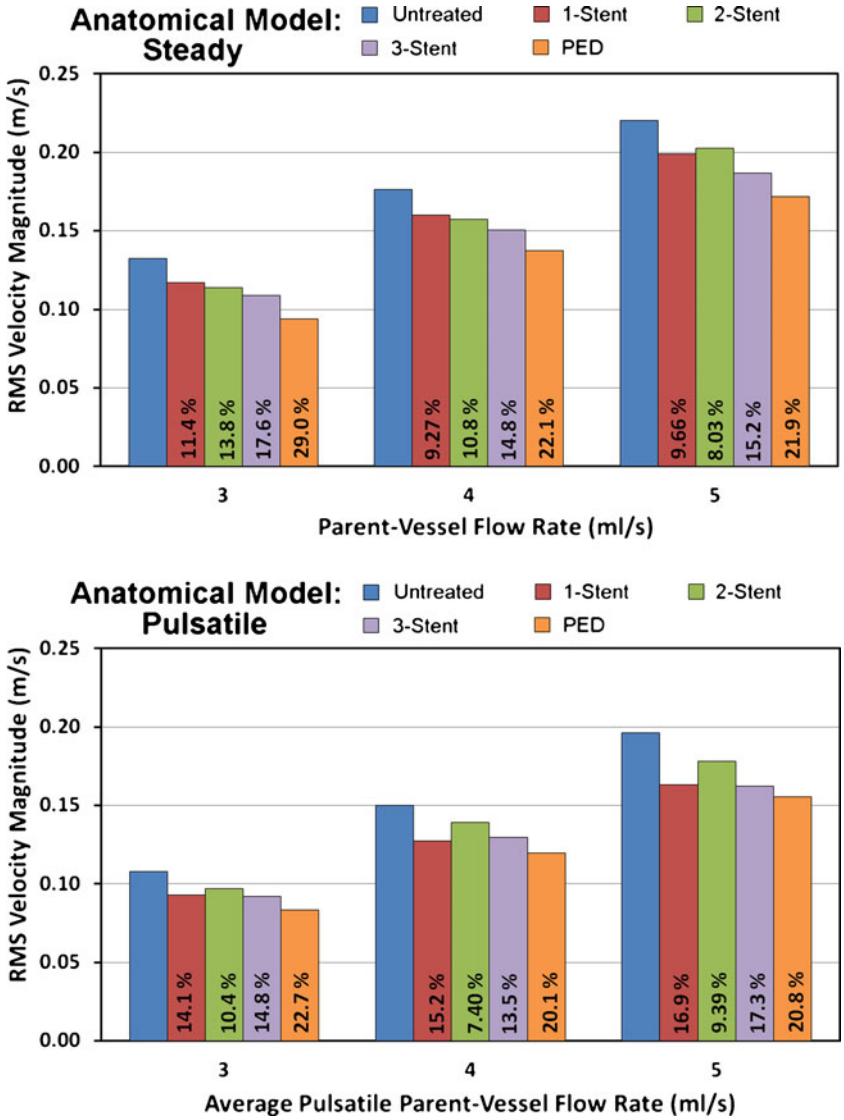

Fig 2 V_{RMS} within the aneurysm of the patient-specific model for each flow rate and treatment. The tortuous geometry of the patient-specific model led to more variation in the effectiveness of the treatment method

Discussion

Flow diverters have been found effective in treating cerebral aneurysms that are not suitable for treatment with more traditional methods (e.g., coiling, craniotomy, and clipping). However, stand-alone stents and flow diverters are a recent addition to the field of endovascular neurosurgery, and their effects on aneurysmal hemodynamics are not yet well understood. This study applied in vitro techniques to measure the effects of stents and flow diverters on aneurysm hemodynamics in order to enhance current understanding of the devices and how they can best be used to treat cerebral aneurysms.

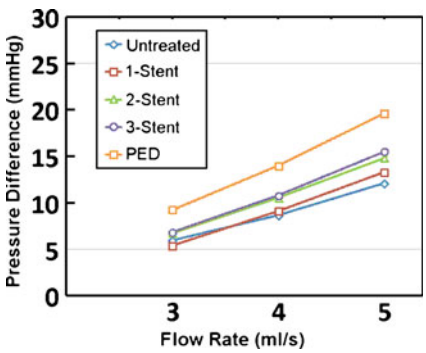

Fig 3 Pressure difference across the patient-specific model, which is the difference between the pressure at the inlet and the pressure at the untreated outlet. The increase in pressure difference with the use of the PED indicates an increase in resistance to the untreated side

As expected, deployment of each device in our experiments led to reductions in fluid dynamic activity within the aneurysm; however, there were obvious differences between effects in the idealized and patient-specific model flows. For the idealized case, sequential placement of telescoping high-porosity stents resulted in increased V_{RMS} reductions as each stent was deployed. Reductions in V_{RMS} with sequential stent placements were not linear, which was expected since the placement of telescoping stent cells relative to one another was not regulated (other than ensuring that the stent struts were not directly aligned). Accordingly, the changes in

porosity that occurred with each stent deployment were unregulated. A previous in vitro study by our group investigated telescoping Neuroform stents across an idealized sidewall aneurysm, which resulted in a similar pattern of reductions in V_{RMS} as each stent was deployed [14]. The results reported here also agree with a computational study by Tremmel et al. [15] that looked at stent-in-stent deployments of Enterprise stents. As in our study, Tremmel found that with each sequential stent deployment, there was a reduction in fluid dynamic activity within the aneurysm; however, their study was based on both decreases in wall shear stress and average velocity magnitude [15].

In contrast to the idealized model, V_{RMS} in the patient-specific model increased with the two-stent deployment when compared to the one-stent deployment. The reason for the increase is from the tortuous patient-specific geometry, which forced the high-porosity stent to bend at an acute angle. As shown in Fig. 4, the bending of the stent leads to what is often described as a "fish mouth" shape common to open-cell stent designs, which in this case forms a jet that is directed into the aneurysm. The jet is highlighted in the flow maps corresponding to the one- and two-stent deployments in Fig. 4. With the three-stent deployment, the jet begins to dissipate and once again the V_{RMS} within the aneurysm is reduced. In contrast, Fig. 5 shows that the vessel geometry of the idealized case leads to a uniform deployment of the stents within the parent vessel, which prohibits the formation of jets, such as the one observed in the patient-specific model.

The discrepancies between stent performance in the idealized and patient-specific cases highlight the important role that vessel and aneurysm geometry can play in the effective placement of stents or flow diverters and the corresponding fluid dynamics. Similar findings were reported in a recent in vivo study by Darsaut et al. [20] that compared the effectiveness of flow diverters in treating three types of surgically created aneurysms in canines. That study found that flow diverters were effective in occluding straight sidewall aneurysms, but were not as effective in treating curved sidewall or end-wall basilar-type aneurysms due to the more tortuous geometries of the aneurysm vessels, which promote more complex diverter shapes and positions [20]. Our observations agree with the results of Darsaut et al., which indicate that changes in flow diverter shape (e.g., malposition) due to vessel geometry lead to significant hemodynamic changes within the aneurysmal sac, which, in turn, could reduce the effectiveness of the device in occluding the aneurysm.

In contrast to the low-porosity stent, the PED showed better flexibility and adhesion to vessel walls when deployed in the patient-specific model. Shown in Fig. 4, the PED was not affected by the acute angle of the vessel. High-porosity stents attempt to provide such flexibility with an open-cell design that facilitates navigation through tortuous vessels; however, when open-cell designs are bent at extreme angles (which occurred in the patient-specific model examined here), the stent struts can actually protrude into the aneurysm, causing unfavorable hemodynamics [21].

In both the idealized and patient-specific models, the PED led to the greatest reductions in fluid dynamic activity within the aneurysm. The superior reduction is likely a combination of the lower porosity and the more effective deployment shape. However, it should be noted that the differential in average V_{RMS} reduction between the three-stent deployment and the PED was marginal, only 8 and 4 % for the steady and pulsatile flow, respectively. The results presented here are similar to our previous in vitro study of an idealized sidewall aneurysm, where the difference between three telescoping stents and the PED was negligible [14]. The similarity between the two deployments has important implications because, in some cases, the use of a PED may not be possible, especially if the aneurysm has been treated previously. For example, aneurysms that have been treated in the past with stent-assisted coiling and reoccurred can be treated with limited options (e.g., adding more coils or surgical clipping). In such cases, there are concerns that treatment with a PED would not be effective because it will appose poorly and lead to possible "endo-leaks"

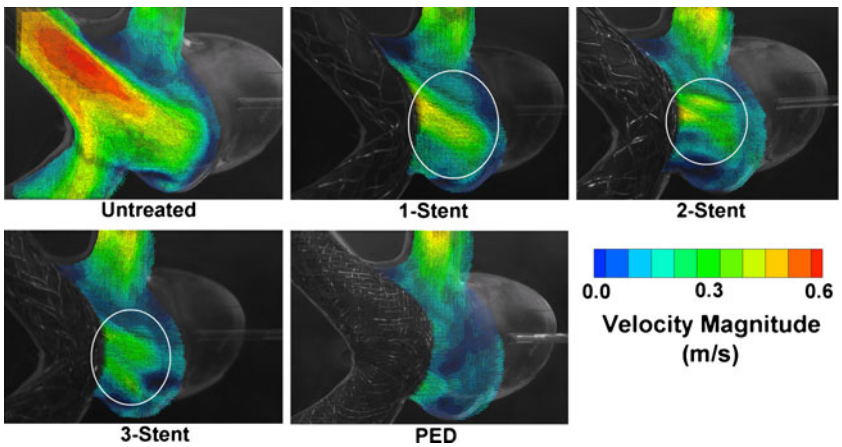

Fig 4 Velocity vector maps describing a representative plane from the patient-specific model for a 4-ml/s steady flow rate. Each configuration is labeled. *Highlighted in white* is the jet formed with the deployment of the high-porosity stents

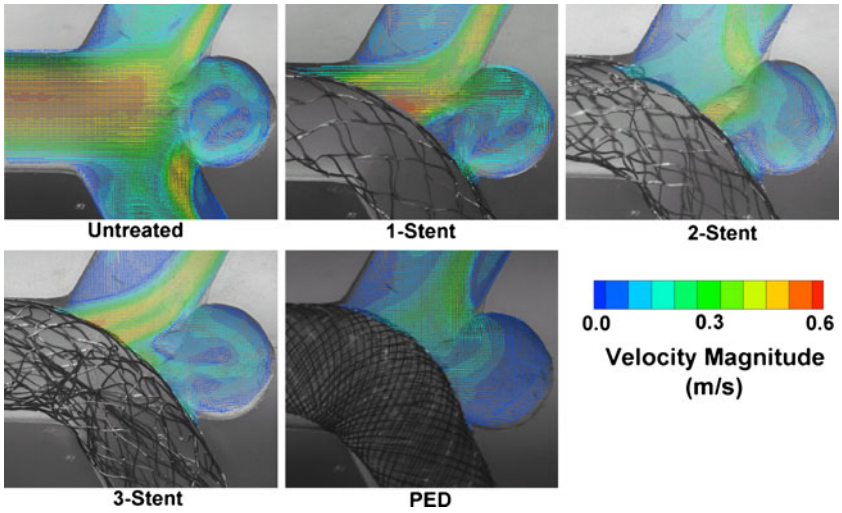

Fig 5 Velocity vector maps describing the center plane of the idealized model for a 4-ml/s steady flow rate. Each configuration is labeled

[11 ,22]. An increased difficulty in navigating the PED into position for deployment has also been observed when an aneurysm has been previously treated with a stent [11]. The increased pore density also may limit the ability of adding additional coils later, if necessary. However, adding a more porous stent to the previous construct allows for a better configuration and still allows for the use of additional coils to assist in the aneurysm occlusion, if necessary.

Pressure measurements taken within the aneurysm fluctuated within 1 or 2 mmHg as the flow rate increased, regardless of treatment. Such small changes are consistent with previous findings from computational studies wherein reductions in flow within the aneurysm did not lead to significant changes in intra-aneurysmal pressure [14 ,23]. However, the pressure differential between the inlet and untreated outlet, which is also the pressure difference across the model, did change with each treatment configuration. As shown in Fig. 3, the pressure difference across the model increased with each sequentially placed stent, and the PED caused the greatest pressure difference of all. The increases in pressure difference show that device deployment leads to alterations in flow resistance through the untreated side of the model, indicating that flow may be preferentially diverted through deployed devices. Variations in pressure differences with different device configurations are also informative because they show that flow through high-porosity stents increased with each sequential placement, even though intra-aneurysmal fluid dynamic activity fluctuated. Such findings emphasize the impact of the flow activity near the aneurysm, which was affected by the diverter deployment shape in the patient-specific aneurysm model.

It should be noted that physiologic pressure drops were employed across the models explored in this study rather than physiologic absolute pressures; that is, pressures at the model inlets and outlets were not maintained so as to represent physiological conditions in an absolute sense (which can pose additional experimental challenges), but were configured instead to use physiologic pressure drops across the models. In a fundamental study by Conrad [24] describing the flow in collapsible tubes, he found that flow was in fact a function of pressure drop and concluded "The pressure drop between the inlet and outlet determines the flow." For studies like the one presented here, such pressure drops facilitate recreation of realistic in vivo flow regimes and may in fact be more of a concern than absolute pressures in performing experiments like ours effectively. Specifically, pressure drops across our system were near 40 mmHg for each flow rate, which is within the physiologic range observed in the cerebrovascular system in vivo. A recent and well-received study by Dorn et al. [25] used similar methods to observe the effects of flow diverters on hemodynamics within sidewall cerebral aneurysms. The pulsatile conditions, blood analog fluids, and matched pressure drops used in our experiments agree well with that study, among others, although Dorn et al. also chose to match absolute pressures to physiologic conditions.

Several limitations of this study relate to the amount of experiments that could be run in an efficient and time-effective manner. While the flow rates, models, and deployment geometries chosen represent only a few of the many clinical possibilities, we feel that the cases selected comprise a representative cross-section of bifurcation aneurysm conditions and thus provide a strong foundation for assessing trends. Furthermore, results of the study could potentially serve as templates for predicting general fluid dynamics in aneurysmal geometries similar to those examined here since geometry has been established as a primary factor that determines fluid dynamics. Our study was also limited in that only two hemodynamic properties, V_{RMS} and pressure, were considered. However, we feel that these metrics are well defined and also characterize the overall hemodynamics within the aneurysm well. Future study goals include developing improved computational models of patient-specific geometries (to include wall compliance), advancing

computational modeling of stents and flow-diverting devices, and further characterizing the effects of vascular geometry and different flow diversion treatments on aneurysmal fluid dynamics using both experimental and computational techniques.

Conclusions

Overall, the low-porosity PED led to greater reductions in intra-aneurysmal fluid dynamic activity than telescoping high-porosity stents. However, in cases where PED deployment may not be an option, sequential telescoping of multiple high-porosity stents can still lead to considerable reductions in intra-aneurysmal fluid dynamic activity, especially in comparison to a single high-porosity stent. Flexibility of the PED also led to better deployment in the tortuous vessels of our patient-specific aneurysm model. The results of this study demonstrated the important effects that different stent and flow diversion treatments can have on hemodynamic outcomes in bifurcating aneurysms.

Acknowledgments This work was supported in part by the following sources: Brain Aneurysm Foundation Research Grant, Women and Philanthropy Society Category B Grant, American Heart Association Beginning Grant in Aid, and National Science Foundation CAREER Award.

Conflict of interest We declare that we have no conflict of interest.

References

1. Higashida RT, Lahue BJ, Torbey MT, Hopkins LN, Leip E, Hanley DF (2007) Treatment of unruptured intracranial aneurysms: a nationwide assessment of effectiveness. Am J Neuroradiol 28:146–151
2. International Subarachnoid Aneurysm Trial (ISAT) Collaborative Group (2002) International Subarachnoid Aneurysm Trial (ISAT) of neurosurgical clipping versus endovascular coiling in 2143 patients with ruptured intracranial aneurysms: a randomized trial. Lancet 360:1267–1274
3. Molyneux AJ, Kerr RSC, Birks J, Ramzi N, Yarnold J, Sneade M, Rischmiller J (2005) International Subarachnoid Aneurysm Trial (ISAT) of neurological clipping versus endovascular coiling in 2143 patients with ruptured intracranial aneurysms: a randomized comparison of effects on survival, dependency, seizures, rebleeding, subgroups, and aneurysms occlusion. Lancet 366:809–817
4. Murayama Y, Nien Y, Duckwiler G, Gobin YP, Jahan R, Frazee J, Martin N, Vineula F (2003) Guglielmi detachable coil embolization of cerebral aneurysms: 11 years' experience. J Neurosurg 98:959–966
5. Gaughen JR, Hasan D, Dumont AS, Jensen ME, Mckenzie J, Evans AJ (2010) The efficacy of endovascular stenting in the treatment of supraclinoid internal carotid artery blister aneurysms using a stent-in-stent technique. AJNR 31:1132–1138
6. Fiorella D, Albuquerque FC, Deshmukh VR, Woo HH, Rasmussen PA, Masaryk TJ, McDougall CG (2006) Endovascular reconstruction with the Neuroform stent as monotherapy for the treatment of uncoilable intradural pseudoaneurysms. Neurosurgery 59(2):291–300
7. Fiorella D, Albuquerque FC, Han P, McDougall CG (2004) Preliminary experience using the Neuroform stent for the treatment of cerebral aneurysms. Neurosurgery 54:6–17
8. Fiorella D, Albuquerque FC, Deshmukh VR, McDougall CG (2005) Usefulness of the Neuroform stent for the treatment of cerebral aneurysms: results at initial (3–6-mo) follow-up. Neurosurgery 56:1191–1202
9. Pumar JM, Lete I, Pardo MI, Vazquez-Herrero F, Blanco M (2008) LEO stent monotherapy for the endovascular reconstruction of fusiform aneurysms of the middle cerebral artery. AJNR 29:1775–1776
10. Levy DI, Ku A (1997) Balloon-assisted coil placement in wide-necked aneurysms: technical note. J Neurosurg 86:724–727
11. Lylyk P, Miranda C, Ceratto R, Ferrario A, Scrivano E, Luna HR, Berez AL, Tran Q, Nelson PK, Fiorella D (2009) Curative endovascular reconstruction of cerebral aneurysms with the Pipeline embolization device: the Buenos Aires experience. Neurosurgery 64:632–642
12. Wong G, Kwan M, Ng R, Yu S, Poon W (2011) Flow diverters for treatment of intracranial aneurysms: current status and ongoing clinical trials. J Clin Neurosci 18:737–740
13. Canton G, Levy DI, Lasheras JC, Nelson PK (2005) Flow changes caused by the sequential placement of stents across the neck of sidewall cerebral aneurysms. J Neurosurg 103:891–902
14. Roszelle BN, Babiker MH, Hafner W, Gonzalez F, Albuquerque F, Frakes DH (2012) In vitro and in silico study of intracranial stent treatments for cerebral aneurysms: effects of perforating vessel flows. J NeuroIntervent Surg. doi:10.1136/neurintsurg-2012-010322
15. Tremmel M, Xiang J, Natarajan SK, Hopkins LN, Siddiqui AH, Levy EI, Meng H (2010) Alteration of intraaneurysmal hemodynamics for flow diversion using enterprise and vision stents. World Neurosurg 74(2/3):306–315
16. Frakes D, Pekkan K, Dasi L, Kitajima H, Zelicourt D, Leo HL, Carberry J, Sundereswaran K, Simon H, Yoganathan A (2008) Modified control grid interpolation for the volumetric reconstruction of fluid flows. Exp Fluids 45:987–997
17. Frakes DH, Conrad CP, Healy TM, Monaco JW, Fogel M, Sharma S, Smith MJT, Yoganathan AP (2003) Application of an adaptive control grid interpolation technique to morphological vascular reconstruction. IEEE Trans Biomed Eng 50(2):197–206
18. Ford MD, Alperin N, Lee SH, Holdsworth DW, Steinman DA (2005) Characterization of volumetric flow rate waveforms in the normal internal carotid and vertebral arteries. Physiol Meas 26:477–488
19. Babiker H, Gonzalez LF, Albuquerque F, Collins D, Elvikis A, Frakes D (2010) Quantitative effects of coil packing density on cerebral aneurysm fluid dynamics: an in vitro steady flow study. Ann Biomed Eng 38(7):2293–2301
20. Darsaut TE, Bing F, Salazkin I, Gevry G, Raymond J (2012) Flow diverters failing to occlude experimental bifurcation or curved sidewall aneurysms: an in vivo study in canines. J Neurosurg 117:37–44
21. Shobayashi Y, Tanoue T, Tateshima S, Tanishita K (2010) Mechanical design of an intracranial stent for treating cerebral aneurysms. Med Eng Phys 32:1015–1024
22. Fiorella D, Lylyk P, Szikora I, Kelly ME, Albuquerque FC, McDougall CG, Nelson PK (2009) Curative cerebrovascular reconstruction with the Pipeline embolization device: the emergence of definitive endovascular therapy for intracranial aneurysms. J NeuroInterv Surg 1:56–65
23. Lieber B, Gounis M (2002) The physics of endoluminal stenting in the treatment of cerebrovascular aneurysms. Neuro Res 24:33–42
24. Conrad W (1969) Pressure flow relationships in collapsible tubes. IEEE Trans Biomed Eng 16:284–295
25. Dorn F, Niedermeyer F, Balasso A, Liepsch D, Liebeg T (2011) The effect of stents on intra-aneurysmal hemodynamics: in vitro evaluation of a pulsatile sidewall aneurysm using laser Doppler anemometry. Neuroradiology 53:267–272